AAS 22-624

OPTIMAL CONTROL IN THE CIRCULAR RESTRICTED THREE-BODY PROBLEM USING INTEGRATION CONSTANTS

Walter J. Manuel* **and Simone D'Amico†**

This paper presents a method for spacecraft to transfer between halo orbits at the optimal delta-v cost. Halo orbits are three-dimensional periodic orbits that form in the Circular Restricted Three-Body Problem (CR3BP). CR3BP motion can be decomposed, expanded to extract more linear terms, and then parameterized to use integration constants (IC) as state variables. By incorporating reachable set theory, the IC can be used to achieve optimal control via an impulsive solver. This helps fill the current gaps in the state-of-the-art by approaching optimal control in a way that is potentially better suited for new and emerging spacecraft trajectory design requirements, specifically more frequent reconfiguration. This will allow spacecraft to enter multiple halo orbits over the course of their lifetime, opening the door to achieve more science objectives. The optimality of the impulsive solution is evaluated against a new delta-v lower bound based on the system energy. The proposed method is also compared to a version of itself that does not include the additional linear terms, in order to demonstrate the advantages of this approach.

INTRODUCTION

The Circular Restricted Three-Body Problem (CR3BP) can open the door to diverse trajectories capable of enabling mission objectives not previously possible. However, the nonlinear dynamics and chaotic behavior present in the CR3BP and near libration points make it difficult to analyze. Thus, many related topics with potential benefits for space exploration as a whole, but especially astrophysics and earth science missions, have still not been widely explored. A halo orbit, which is a three-dimensional periodic orbit that can form in the vicinity of a libration point, could have several advantages to the mission over a two-body orbit. For example, halo orbits can yield both more and longer observation opportunities as the spacecraft naturally moves through 360 degrees of right ascension, decreasing the costs and frequency of reconfiguration maneuvers.[1] Typical missions thus far set a single nominal halo orbit for their duration. However, more opportunity for science would be opened if missions were able to efficiently reconfigure between different halo orbits, especially as this would allow access to broader declinations. When a spacecraft is aligned in formation with another spacecraft or the Earth, it is constrained by the position vector between the two bodies, and therefore attitude rotation alone is not sufficient to facilitate goals such as viewing specified inertial targets. In order to have access to most or all 180 degrees of declination, thus making the majority of the field of inertial targets, such as stars, available for viewing, the spacecraft must be able to change to different halo orbits. The main goal of this paper is to present a method to transfer between halo orbits at the optimal delta-v cost. Reducing the reconfiguration costs associated with halo orbits

*Graduate Student, Department of Aeronautics and Astronautics, Stanford University, Stanford, CA 94305.
†Associate Professor, Department of Aeronautics and Astronautics, Stanford University, Stanford, CA 94305.

will help increase their viability and allow their advantages to actually be realized for modern space science missions.

While this work could be applied in many ways, one specific area is simultaneous alignment of a spacecraft with an inertial target and a ground telescope. This is an objective that has little precedent based on current literature, and there is even less existing work on inertial alignment for spacecraft in halo orbits.[1] One such mission proposed by NASA Goddard Space Flight Center (GSFC) in collaboration with Stanford's Space Rendezvous Laboratory (SLAB) is the Orbiting Configurable Artificial Star (ORCAS), which aims to launch a spacecraft (the artificial guide star) that can simultaneously align in the field of view of the ground-based observatory and with an inertial observation target (such as a star). The goal of the ORCAS mission is to allow ground-based observatories on Earth to take higher quality images using adaptive optics.[2] The spacecraft's laser will be pointed back towards the ground-based Earth observatory, where the received signal can be used to help correct images, effectively making the spacecraft an artificial guide star. ORCAS and SLAB researchers have noted that, when compared to high elliptical orbits (the nominal orbit design choice for ORCAS), halo orbits would offer more potential in viewing multiple stars using a single orbit, could significantly reduce the fuel cost, and should be considered for future missions with similar requirements to those of ORCAS.[3] A similar mission proposed by GSFC, with contributions from SLAB, is the Orbiting Starshade (OS), which features a starshade in lieu of the artificial guide star.[4] The techniques described in this paper could allow missions such as ORCAS and OS to view more inertial targets along multiple orbits over the mission lifetime, while still conserving delta-v.

Several methods exist for transferring between halo orbits. Hiday-Johnston and Howell used primer vectors and an unconstrained optimization solver to generate optimal time-free transfers[5,6] and time-fixed transfers.[7] Gomez et al. derived a different two-impulse transfer method for halo orbits about the same libration point by exploiting the Floquet nodes associated with each halo orbit.[8] Single and multiple shooting techniques have been used to find locally optimal transfer trajectories between halo orbits at the same libration point, and have also been used in literature to generate a reference trajectory to compare new results to.[9] Also of relevance are methods that have been used to find analytical solutions or approximations for halo orbits. The most commonly cited analytical solution is Richardson's third-order expansion.[10] A set of linearized equations of motion can be obtained through a similar process, and have been used to generate approximations of halo orbits as well.[1] In the area of optimal control and reconfiguration, a relevant method is that of integration constants. Motion can be modeled as a weighted sum of fundamental solutions and parameterized to use integration constants (IC) as state variables.[11] This approach has recently been applied to both Keplerian and CR3BP relative motion, but not to CR3BP absolute motion.[12] IC provide an avenue to simplify the motion and incorporate optimal control via impulsive optimization algorithms grounded in reachable set theory.

Limitations exist in the state-of-the-art for halo-to-halo transfers, thus motivating the need for improved transfer methods. For example, the methods described above only consider two-impulse and three-impulse transfers, but it is possible that more cost-optimal trajectories could be found if the number of impulses is allowed to vary. Also, the time-free methods might not be suitable for future space missions with specific timing requirements, such as missions where the spacecraft must reconfigure its orbit so that it is aligned with an inertial target at the correct time. Furthermore, the method by Gomez et al. was designed for transferring from larger to smaller halo orbits in a scenario where the spacecraft first launches from Earth to the larger halo orbit, so it may not have the flexibility to accommodate all types of transfers.[8] Incorporating reachable set theory and

the IC method could help fill these gaps by producing an approach to optimal control that is more general and better suited for new and emerging spacecraft trajectory design requirements. Missions like ORCAS that will use multiple orbits over the duration of their lifetime would benefit from the ability to repeatedly reconfigure at the optimal cost. The IC and reachable set approaches have already found success in other applications, such as multi-agent passive safety using IC,[13] or formation flying control via reachable set theory,[14] but the usage of IC to model CR3BP motion is a new direction, as existing state-of-the-art on halo orbit transfers primarily leveraged primer vector theory[5] and Floquet theory.[8]

This paper is organized into three main sections. First, mathematical background on the CR3BP is given to understand the terminology and concepts germane to the problem formulation. Second, a new approach based on the integration constants method is presented, featuring two contributions to the state-of-the-art. The IC method is applied to the CR3BP after first using Legendre polynomials to expand the original equations of motion to include more linear terms. Also, a new technique for forming upper and lower bounds on the delta-v cost of halo orbit reconfiguration is derived, which can be used to validate the IC method. In the third main section, the approach is evaluated in three ways. To demonstrate the ability of the IC method to produce a trajectory using a reachable set impulsive solver, graphical and numerical results from a hypothetical transfer trajectory are presented. Next, to evaluate the optimality of such trajectories produced by the solver, delta-v costs of multiple transfer trajectories are compared to the newly derived upper and lower bounds. And finally, to support the rationale for expanding out the equations of motion in the approach, an accuracy comparison is made to a reapplication of the IC method using the original, unexpanded equations of motion.

BACKGROUND ON THE CR3BP

Mathematical background knowledge is provided in this section on the key properties of the CR3BP, so that the dynamics of a halo orbit transfer can be properly understood. In the CR3BP setup, there are two bodies of significant mass, such as stars, planets, or moons, accompanied by a spacecraft of negligible mass.[15] The two larger bodies rotate in circular, equatorial orbits about their common center of mass. In order to analyze motion in the CR3BP system, it is usually necessary to nondimensionalize its quantities and express them in a Synodic Rotating Frame (SRF), which is a reference frame that is centered at the barycenter between the two primaries, and has the same inertial angular velocity as the primaries. In the right-handed SRF, the x-axis is defined along the direction from the first primary to the second primary, the y-axis is within the plane of motion of the two primaries and perpendicular to the x-axis, and the z-axis points perpendicularly out of the plane of motion of the two primaries. A visualization of the SRF is shown in Figure 1.

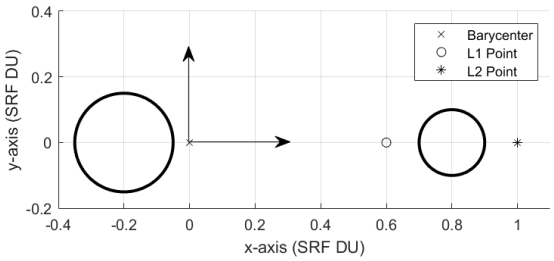

Figure 1. Diagram of SRF for arbitrary system with 1st primary represented by the larger circle and 2nd primary by the smaller circle. The z-axis points out of the page.

There are five stationary points in the SRF at which the gravitational and centrifugal forces in the system are balanced. These points are known as either Lagrange points or libration points, and are often abbreviated as L1, L2, etc. It is possible to place spacecraft in three-dimensional periodic orbits about the libration points called halo orbits.

In the CR3BP, the three bodies are modeled as point masses. The two larger bodies with non-negligible mass are referred to as the first primary and second primary, or sometimes as the primary and the secondary, and have masses denoted as m_1 and m_2 respectively. Mass m_1 is greater than mass m_2, and the masses can be related by the mass parameter μ given by

$$\mu = \frac{m_2}{m_1 + m_2} \tag{1}$$

For the nondimensionalized system, the unit of mass is the total mass of the system (m_1+m_2), the unit of length is the distance between the centers of the primaries, and the unit of time is chosen so that orbital period of the rotating system about its barycenter is 2π. Under this framework, the mean motion and the gravitational parameter GM (the product of the Newtonian gravitational constant G and the mass M of the bodies, not to be confused with the CR3BP mass parameter μ) are also equal to 1. In this section, the coordinates $\bar{x}$, $\bar{y}$, and $\bar{z}$ refer to non-dimensionalized coordinates in the SRF.

Some key quantities in the CR3BP are the effective potential (also known as the pseudo-potential) U, and the Jacobi constant C_J. The pseudo-potential incorporates both standard gravitational potential energy and the centrifugal force induced by the rotating reference frame, as

$$U = \frac{1}{2}(\bar{x}^2 + \bar{y}^2) + \frac{(1-\mu)}{d_1} + \frac{\mu}{d_2} \tag{2}$$

Here, d_1 is the distance from the spacecraft to the large primary, and d_2 is the distance from the spacecraft to the small primary, given by

$$d_1 = [(\bar{x} + \mu)^2 + \bar{y}^2 + \bar{z}^2]^{1/2} \tag{3}$$
$$d_2 = [(\bar{x} - 1 + \mu)^2 + \bar{y}^2 + \bar{z}^2]^{1/2} \tag{4}$$

The Jacobi constant equals $-2E$, where E is the total effective energy given by the sum of effective kinetic and potential energies as

$$E = -U + \frac{1}{2}(\dot{\bar{x}}^2 + \dot{\bar{y}}^2 + \dot{\bar{z}}^2) \tag{5}$$
$$C_J = 2U - (\dot{\bar{x}}^2 + \dot{\bar{y}}^2 + \dot{\bar{z}}^2) \tag{6}$$

E, and therefore C_J, are both conserved in the SRF. In general, the Jacobi constant is the only integral constraining the motion of the spacecraft in the CR3BP.[16] Note that there is a distinction between "integrals of motion" and "motion constants", as defined in classical mechanics.[17] For an

nth-order autonomous system, n state and time-dependent integrals of motion exist, and up to $n-1$ time-independent motion constants exist. The quantities referred to as integration constants in this work are an example of the former, while the Jacobi constant is an example of the latter.

The nonlinear CR3BP equations of motion (EOMs) are given by

$$\ddot{\bar{x}} - 2\dot{\bar{y}} = \frac{\partial U}{\partial \bar{x}} \tag{7}$$

$$\ddot{\bar{y}} + 2\dot{\bar{x}} = \frac{\partial U}{\partial \bar{y}} \tag{8}$$

$$\ddot{\bar{z}} = \frac{\partial U}{\partial \bar{z}} \tag{9}$$

They are non-integrable analytically and thus do not have known closed form solutions.

Another coordinate frame commonly used when studying the CR3BP is the Rotating Libration Point Frame (RLPF). The RLPF transformation simply moves the origin to the libration point of interest, and also scales the coordinate system so that the distance between the libration point of interest and the small primary is 1. This transformation can be computed as

$$x = \frac{\bar{x} - 1 + \mu \pm \gamma}{\gamma} \tag{10}$$

$$y = \frac{\bar{y}}{\gamma} \tag{11}$$

$$z = \frac{\bar{z}}{\gamma} \tag{12}$$

$$\tag{13}$$

Here, the constant γ denotes the distance from the libration point to the smaller primary in the SRF, and the normalized state variables in the RLPF are represented as x, y, and z. A visualization of the RLPF is shown in Figure 2.

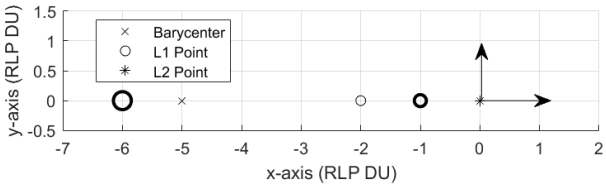

Figure 2. Diagram of RLPF for arbitrary system with 1st primary represented by the larger circle and 2nd primary by the smaller circle. The z-axis points out of the page.

The last key piece of background information that is relevant for this paper is the concept of halo orbit families. Halo orbits occur in clusters known as families around each libration point. These families, which are symmetric about the x and z axes in the SRF, can be generated using continuation schemes, as described in literature.[18] This paper examines how to transfer between halo orbits in the Sun-Earth L2 halo orbit family, which is the one most applicable to the ORCAS mission.[1] This family of halo orbits is illustrated in Figure 3.

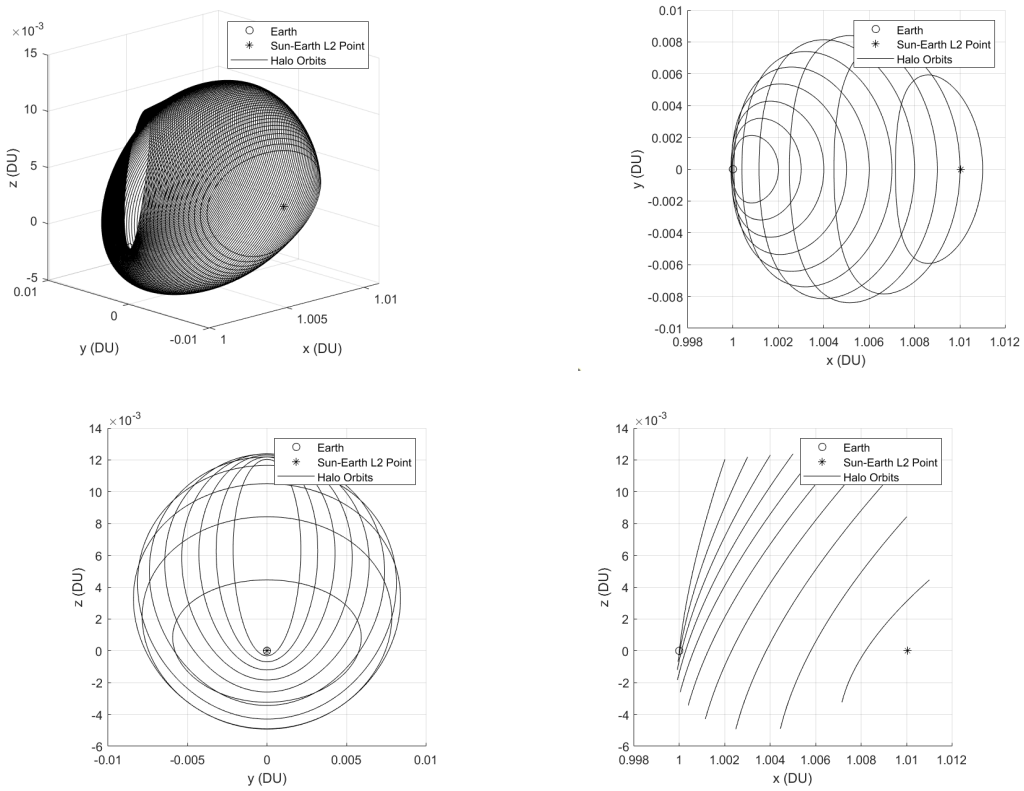

Figure 3. Northern Family of Sun-Earth L2 Halo Orbits, shown in 3D (top left), xy-plane (top right), yz-plane (bottom left), and xz-plane (bottom right) views. Family is generated via a continuation scheme and plotted in SRF nondimensional coordinates.

NEW APPROACH BASED ON INTEGRATION CONSTANTS

The novel approach presented in this paper takes a first step towards applying the integration constants method to CR3BP motion using the expansion and linearization methods developed by Richardson, and demonstrates how IC space provides avenues to incorporate optimal control by leveraging reachable set theory. The approach consists of three main portions. First, the spacecraft motion is decomposed into linear and nonlinear parts. Second, the linear part is solved analytically to derive a closed-form map between the original state variables and the IC. Third, control terms are added as perturbations in order to incorporate optimization into the method. Finally, a new metric for computing delta-v upper and lower bounds based on the Jacobi constant is derived so that the optimality of solutions can be evaluated.

Integration Constants in the CR3BP

The spacecraft position and velocity expressed in the SRF are combined in the spacecraft motion vector $\boldsymbol{X}(t) \in \mathbb{R}^6$. $\boldsymbol{X}(t)$ is driven by a set of 6 non-integrable first-order ordinary differential equations (ODEs), $\boldsymbol{F}(t, \boldsymbol{X})$, that can be separated as follows

$$\dot{\boldsymbol{X}}(t) = \boldsymbol{F}(t, \boldsymbol{X}) = \boldsymbol{F}'(t, \boldsymbol{X}) + \boldsymbol{F}_p(t, \boldsymbol{X}) \tag{14}$$

where $\boldsymbol{F}'(t, \boldsymbol{X})$ is the integrable part of the ODEs, and $\boldsymbol{F}_p(t, \boldsymbol{X})$ is the non-integrable part.[11]

The nonlinear and non-integrable CR3BP EOMs, previously introduced in Equations (7)-(9), are reproduced in an equivalent form with the pseudo-potential terms expanded as

$$\ddot{\bar{x}} - 2\dot{\bar{y}} - \bar{x} = -\frac{(1-\mu)(\bar{x}+\mu)}{{d_1}^3} - \frac{\mu(\bar{x}+\mu-1)}{{d_2}^3} \tag{15}$$

$$\ddot{\bar{y}} + 2\dot{\bar{x}} - \bar{y} = -\frac{(1-\mu)\bar{y}}{{d_1}^3} - \frac{\mu\bar{y}}{{d_2}^3} \tag{16}$$

$$\ddot{\bar{z}} = -\frac{(1-\mu)\bar{z}}{{d_1}^3} - \frac{\mu\bar{z}}{{d_2}^3} \tag{17}$$

Equations (15)-(17) is the system of ODES that must be separated in order to use the IC method. In order to have more linear terms in the EOMs, it is convenient to convert the coordinates to the RLPF. This coordinate conversion will allow the nonlinear EOMs to be expanded using Legendre polynomials following the procedure outlined by Richardson,[10] which yields an approximate form given by

$$\ddot{x} - 2\dot{y} - (1+2c_2)x = \sum_{n=2}^{\infty}(n+1)c_{n+1}\rho^n P_n(x/\rho) \tag{18}$$

$$\ddot{y} + 2\dot{x} + (c_2-1)y = \sum_{n=3}^{\infty} c_n y \rho^{n-2}\tilde{P}_n(x/\rho) \tag{19}$$

$$\ddot{z} + c_2 z = \sum_{n=3}^{\infty} c_n z \rho^{n-2}\tilde{P}_n(x/\rho) \tag{20}$$

The left-hand-side (LHS) of Equations (18)-(20) represents the linear, integrable part of the CR3BP EOMs and the right-hand-side (RHS), consisting of higher order polynomial terms, represents the non-integrable part. The scalar ρ is the magnitude of the position vector of the spacecraft relative to the libration point, and the quantity P_n denotes the nth Legendre polynomial. The Legendre constants c_n are not to be confused with the integration constants (C_i), and are given by

$$c_n = \frac{1}{\gamma^3}\left((\pm 1)^n\mu + (-1)^n\frac{(1-\mu)\gamma^{n+1}}{(1\mp\gamma)^{n+1}}\right) \tag{21}$$

The quantity $\tilde{P}_n(x/\rho)$ in Equations (18)-(20) represents the sum

$$\tilde{P}_n(x/\rho) = \sum_{k=0}^{(n-2)/2}(3+4k-2n)P_{n-2k-2}(x/\rho) \tag{22}$$

The integrable part, often denoted as the linearized CR3BP EOMs, is written in matrix form as

$$\boldsymbol{F}'(t,\boldsymbol{X}) = \dot{\boldsymbol{X}}'(t) = \begin{bmatrix} \dot{x} \\ \dot{y} \\ \dot{z} \\ \ddot{x} \\ \ddot{y} \\ \ddot{z} \end{bmatrix} = \begin{bmatrix} 0 & 0 & 0 & 1 & 0 & 0 \\ 0 & 0 & 0 & 0 & 1 & 0 \\ 0 & 0 & 0 & 0 & 0 & 1 \\ 1+2c_2 & 0 & 0 & 0 & 2 & 0 \\ 0 & 1-c_2 & 0 & -2 & 0 & 0 \\ 0 & 0 & -c_2 & 0 & 0 & 0 \end{bmatrix} \begin{bmatrix} x \\ y \\ z \\ \dot{x} \\ \dot{y} \\ \dot{z} \end{bmatrix} \tag{23}$$

There are similarities between the plant matrix for the integrable CR3BP EOMs in Equation (23) and that of the Hill-Clohessy-Wiltshire relative motion EOMs,[19] as noted by previous authors.[20] This allows approaches such as the IC method to be applied similarly for both problems when decomposing the motion and optimizing its path.

The non-integrable part of the CR3BP EOMs, expanded out to include all third-order terms, can be written as

$$\boldsymbol{F}_p(t,\boldsymbol{X}) = \dot{\boldsymbol{X}}_p(t) = \begin{bmatrix} \dot{x} \\ \dot{y} \\ \dot{z} \\ \ddot{x} \\ \ddot{y} \\ \ddot{z} \end{bmatrix} = \begin{bmatrix} 0 \\ 0 \\ 0 \\ \frac{3}{2}c_3(2x^2-y^2-z^2) + 2c_4x(2x^2-3y^2-3z^2) + O(4) \\ -3c_3xy + \frac{3}{2}c_4y(4x^2-y^2-z^2) + O(4) \\ \\ -3c_3xz - \frac{3}{2}c_4z(4x^2-y^2-z^2) + O(4) \end{bmatrix} \tag{24}$$

Solving the characteristic equation of the integrable CR3BP plant matrix yields six eigenvalues, designated as λ_i. $\lambda_{1,3,4,6}$ are imaginary with no real part, while $\lambda_{2,5}$ are real with no imaginary part. ω_i will be used to represent the magnitude of the i^{th} eigenvalue. Due to the reciprocal nature of the eigenvalues, $\lambda_1 = -\lambda_4$, $\lambda_2 = -\lambda_5$, and $\lambda_3 = -\lambda_6$, therefore $\omega_1 = \omega_4$, $\omega_2 = \omega_5$, and $\omega_3 = \omega_6$. These eigenvalue magnitudes ω_i, also referred to as eigenfrequencies, are correlated to the period of the orbit. A higher eigenfrequency means the orbit will complete its period faster. κ_1 and κ_2 are constant ratios that are derived from the eigenvectors.

The linear part $\dot{\boldsymbol{X}}'(t)$ from Equation (23) can be integrated analytically to yield a square fundamental solution matrix $\boldsymbol{\Psi}(t) \in \mathbb{R}^{6\text{x}6}$ between $\boldsymbol{X}(t)$ and the integration constants $C_i \in \mathbb{R}$ as

$$\boldsymbol{X}'(t) = \begin{bmatrix} x \\ y \\ z \\ \dot{x} \\ \dot{y} \\ \dot{z} \end{bmatrix} = \boldsymbol{\Psi}(t) \begin{bmatrix} C_1 \\ C_2 \\ C_3 \\ C_4 \\ C_5 \\ C_6 \end{bmatrix} \tag{25}$$

$$\boldsymbol{\Psi}(t) = \begin{bmatrix} \cos\omega_1 t & \sin\omega_1 t & e^{\omega_2 t} & e^{-\omega_2 t} & 0 & 0 \\ -\kappa_1 \sin\omega_1 t & \kappa_1 \cos\omega_1 t & -\kappa_2 e^{\omega t} & \kappa_2 e^{-\omega t} & 0 & 0 \\ 0 & 0 & 0 & 0 & \cos\omega_3 t & \sin\omega_3 t \\ -\omega_1 \sin\omega_1 t & \omega_1 \cos\omega_1 t & \omega_2 e^{\omega_2 t} & -\omega_2 e^{-\omega_2 t} & 0 & 0 \\ -\kappa_1\omega_1 \cos\omega_1 t & -\kappa_1\omega_1 \sin\omega_1 t & -\kappa_2\omega_2 e^{\omega_2 t} & -\kappa_2\omega_2 e^{-\omega_2 t} & 0 & 0 \\ 0 & 0 & 0 & 0 & -\omega_3 \sin\omega_3 t & \omega_3 \cos\omega_3 t \end{bmatrix} \tag{26}$$

Equation (26) shows the physical interpretation of λ_i, the six eigenvalues. There are four purely imaginary eigenvalues which yield four center modes, one positive real eigenvalue that forms a source mode, and one negative real eigenvalue that forms a sink mode. In equation (26), the pair of center modes in columns one and two corresponds to in-plane motion, while the other pair in columns five and six corresponds to out-of-plane motion. The out-of-plane z motion is decoupled from the xy-plane motion. Using the fundamental solution matrix $\boldsymbol{\Psi}(t)$, the IC for a given halo orbit or other CR3BP trajectories can be solved for as a function of the initial position and velocity, $[x_0, y_0, z_0, \dot{x_0}, \dot{y_0}, \dot{z_0}]^\top$ as

$$\boldsymbol{X}'(t_0 = 0) = \begin{bmatrix} x_0 \\ y_0 \\ z_0 \\ \dot{x_0} \\ \dot{y_0} \\ \dot{z_0} \end{bmatrix} = \begin{bmatrix} 1 & 0 & 1 & 1 & 0 & 0 \\ 0 & \kappa_1 & -\kappa_2 & \kappa_2 & 0 & 0 \\ 0 & 0 & 0 & 0 & 1 & 0 \\ 0 & \omega_1 & \omega_2 & -\omega_2 & 0 & 0 \\ -\kappa_1\omega_1 & 0 & -\kappa_2\omega_2 & -\kappa_2\omega_2 & 0 & 0 \\ 0 & 0 & 0 & 0 & 0 & \omega_3 \end{bmatrix} \begin{bmatrix} C_1 \\ C_2 \\ C_3 \\ C_4 \\ C_5 \\ C_6 \end{bmatrix} \tag{27}$$

In order to form halo-type periodic orbits, there are two key steps. First, the fundamental solutions corresponding to non-center modes must be set equal to 0 in order to suppress the divergent source mode. This can be done by setting the integration constants C_3 and C_4 to zero. This simplifies the initial conditions mapping to

$$\boldsymbol{X}'(t_0) = \begin{bmatrix} x_0 \\ y_0 \\ z_0 \\ \dot{x_0} \\ \dot{y_0} \\ \dot{z_0} \end{bmatrix} = \begin{bmatrix} 1 & 0 & 0 & 0 \\ 0 & \kappa_1 & 0 & 0 \\ 0 & 0 & 1 & 0 \\ 0 & \omega_1 & 0 & 0 \\ -\kappa_1\omega_1 & 0 & 0 & 0 \\ 0 & 0 & 0 & \omega_3 \end{bmatrix} \begin{bmatrix} C_1 \\ C_2 \\ C_5 \\ C_6 \end{bmatrix} \tag{28}$$

Secondly, the eigenfrequencies corresponding to the trigonometric modes must be set equal to obtain periodic motion. Without this assumption only quasi-periodic motion could be obtained from the linearized EOMs. The revised fundamental solution matrix is given by

$$\boldsymbol{\Psi}(t) = \begin{bmatrix} \cos\omega_1 t & \sin\omega_1 t & e^{\omega_2 t} & e^{-\omega_2 t} & 0 & 0 \\ -\kappa_1 \sin\omega_1 t & \kappa_1 \cos\omega_1 t & -\kappa_2 e^{\omega_2 t} & \kappa_2 e^{-\omega_2 t} & 0 & 0 \\ 0 & 0 & 0 & 0 & \cos\omega_1 t & \sin\omega_1 t \\ -\omega_1 \sin\omega_1 t & \omega_1 \cos\omega_1 t & \omega_2 e^{\omega_2 t} & -\omega_2 e^{-\omega_2 t} & 0 & 0 \\ -\kappa_1\omega_1 \cos\omega_1 t & -\kappa_1\omega_1 \sin\omega_1 t & -\kappa_2\omega_2 e^{\omega_2 t} & -\kappa_2\omega_2 e^{-\omega_2 t} & 0 & 0 \\ 0 & 0 & 0 & 0 & -\omega_1 \sin\omega_1 t & \omega_1 \cos\omega_1 t \end{bmatrix} \tag{29}$$

It can be noted that C_3 and C_4 can be non-zero while performing control maneuvers, which is why they are still included in the fundamental solution matrix above. However, while the motion is on an actual halo orbit, they must be zero to cancel out the divergent mode and maintain the periodic motion.

Using simple trigonometric transformations, the solutions to the linearized equations can be expressed in phase-amplitude form.[10] This helps give more geometrical and physical meaning to the IC. The amplitude in the x-direction, A_x, is the L2 norm of the vector $[C_1, C_2]$, while the amplitude in the z-direction, A_z, is the L2 norm of the vector $[C_5, C_6]$

$$x = -A_x \cos(\omega_p t + \phi) \tag{30}$$
$$y = \kappa_1 A_x \sin(\omega_p t + \phi) \tag{31}$$
$$z = A_z \sin(\omega_p t + \psi) \tag{32}$$

The IC vary over time according to the perturbative, non-integrable term of the original ODE. This relationship is given by the Integration Constants Variation Equation (ICVE) as follows

$$\dot{\boldsymbol{C}} = \frac{\partial \boldsymbol{C}}{\partial \boldsymbol{X}}(t, \boldsymbol{C}) \boldsymbol{F}_p(t, \boldsymbol{X}) \tag{33}$$

If control maneuvers are considered as perturbations, they too can be incorporated into the ICVE. The control action can be modeled using a vector of RLPF Cartesian impulsive control actions $\boldsymbol{u} \in \mathbb{R}^3$, given by

$$\boldsymbol{u} = \begin{bmatrix} \Delta v_x \\ \Delta v_y \\ \Delta v_z \end{bmatrix} \tag{34}$$

and the RLPF Cartesian control input matrix $\boldsymbol{B}_x \in \mathbb{R}^{6\text{x}3}$, given by

$$\boldsymbol{B_x} = \begin{bmatrix} 0 & 0 & 0 \\ 0 & 0 & 0 \\ 0 & 0 & 0 \\ 1 & 0 & 0 \\ 0 & 1 & 0 \\ 0 & 0 & 1 \end{bmatrix} \tag{35}$$

as well as the inverse of the fundamental solution matrix given in Equation (29), $\boldsymbol{\Psi}(t)^{-1} \in \mathbb{R}^{6\text{x}6}$.

The addition of control results in the following expression for the time derivative of the IC

$$\dot{\boldsymbol{C}} = \frac{\partial \boldsymbol{C}}{\partial \boldsymbol{X}}(t, \boldsymbol{C})\boldsymbol{F}_p(t, \boldsymbol{X}) + \boldsymbol{\Psi}(t)^{-1}\boldsymbol{B}_{\boldsymbol{x}}\boldsymbol{u} \tag{36}$$

If $\boldsymbol{F}_p$ is neglected in order to simplify the CR3BP dynamics, the IC will only vary under the control action. Furthermore, the product of $\boldsymbol{\Psi}(t)^{-1}$ and $\boldsymbol{B}_x$ can be expressed as a single time-dependent term, $\boldsymbol{B}_c(t)$.

Each halo orbit will have its own distinct set of Cartesian initial conditions, and therefore its own distinct set of integration constants $\boldsymbol{C} \in \mathbb{R}^6$. If the initial halo orbit has the IC vector $\boldsymbol{C}_0$, and the target halo orbit has the IC vector $\boldsymbol{C}_1$, let the difference between the two halo orbits in IC space be designated as $\Delta\boldsymbol{C}_{goal}$. Under the assumption that the admissible control action is a discrete sequence of impulses, as well as the previously stated assumption that perturbations are neglected, the IC difference can be expressed as a summation of the required impulsive control maneuvers

$$\Delta\boldsymbol{C}_{goal} = \sum_{i=1}^{N} \boldsymbol{B}_{\boldsymbol{c}}(t_i)\boldsymbol{u}_i \tag{37}$$

In order to optimally transfer between the two halo orbits, the series of maneuvers that achieve the desired IC variation at the lowest possible cost must be found. Solving this optimization problem necessitates the use of an algorithm grounded in reachable set theory, which was introduced by Koenig and D'Amico,[21] and has previously been used for spacecraft formation flying[14] and spacecraft swarms.[11] The goal is to minimize the total delta-v cost J, defined as

$$J = \sum_{i=1}^{N} \|\boldsymbol{u}_i\| \tag{38}$$

Two convex sets are defined in relation to a given maximum cost J: $\mathcal{U}(J)$, the set of all admissible control inputs $\boldsymbol{u}(t)$; and $\mathcal{C}(J)$, the set of all reachable IC variations $\Delta\boldsymbol{C}$. The optimal maneuver sequence, under the simplifying assumption of neglecting the non-integrable terms, can then be solved for using the algorithm described first by Koenig and D'Amico,[21] and also used by Guffanti and D'Amico[11] specifically in the context of IC. This produces a set of maneuver times, directions, and magnitudes.

In summary, this approach consisted of three key steps. First, the CR3BP EOMs were expanded using Legendre polynomials and the linear and nonlinear parts of the CR3BP EOMs were separated out. Third, the linear part was solved analytically to yield a closed-form map of Halo-type motion to IC. Finally, control terms were incorporated which allowed the use of reachable set theory to solve for the optimal control maneuver sequence. Multiple simplifying assumptions were made throughout, including neglecting the non-integrable perturbative part of the EOMs, which is why the approach cannot be considered fully optimal.

However, it still represents a key first step forward, mainly due to the extraction of more linear terms from the EOMs using Richardson's method, which gave a closer approximation of actual halo orbits and periodic motion when deriving the IC, as will be shown in the Results and Evaluation of Approach section. This method was applied in a way that goes beyond its original purpose, which was to construct linear and third order approximations, not to use IC as state variables or incorporate optimal control.[10]

Jacobi Bounds

A typical problem is the evaluation of the optimality of the obtained maneuver plan described in the previous section when applied to the nonlinear EOMs of the CR3BP. This paper develops a simple, yet novel metric based on the energy properties of the CR3BP to find delta-v upper and lower bounds on the cost of transfers between halo orbits. Each halo orbit has its own unique effective orbital energy, and therefore its own Jacobi constant, which means that the maneuvers to transfer between halo orbits must change the Jacobi constant until it matches that of the target halo orbit. By leveraging the definition of the Jacobi Constant from Equation (6), a method to analytically solve for upper and lower bounds on the delta-v magnitude required to switch between halo orbits can be derived. C_{J_1} and C_{J_2} are the Jacobi constants of the starting and ending halo orbits, respectively. The velocity of the spacecraft at any point can be represented by the vector $\boldsymbol{v} \in \mathbb{R}^3$. The velocity at the current point on the starting halo orbit is $\boldsymbol{v}_1$. If position remains constant, the velocity that the spacecraft would need for the effective orbital energy to match that of the ending halo orbit is $\boldsymbol{v}_2$. This means the Jacobi constants of each orbit can be represented by

$$C_{J_1} = 2U - {v_1}^2 \tag{39}$$
$$C_{J_2} = 2U - {v_2}^2 \tag{40}$$

The delta-v required to change from $\boldsymbol{v}_1$ to $\boldsymbol{v}_2$ is $\boldsymbol{v}_t$, as follows

$$\boldsymbol{v_2} = \boldsymbol{v_1} + \boldsymbol{v_t} \tag{41}$$

Substituting Equation (41) into Equation (40) yields the following expression

$$C_{J_2} = 2U - ({v_1}^2 + {v_t}^2 + 2\boldsymbol{v_1} \cdot \boldsymbol{v_t}) \tag{42}$$
$$C_{J_2} = 2U - ({v_1}^2 + {v_t}^2 + 2v_1 v_t \cos\theta) \tag{43}$$

Here, θ denotes the angle between $\boldsymbol{v}_1$ and $\boldsymbol{v}_t$. With further algebraic manipulation, Equation (43) can be put in quadratic form, with v_t as the variable of interest, as

$$0 = {v_t}^2 + 2v_1 v_t \cos\theta + ({v_1}^2 + C_{J_2} - 2U) \tag{44}$$
$$0 = {v_t}^2 + 2v_1 v_t \cos\theta + (C_{J_2} - C_{J_1}) \tag{45}$$

θ can be varied to solve for all possible values of v_t. If θ is set to either 0° or 180°, and the absolute values of the roots of the quadratic equation are found, the larger root will be the upper bound and the smaller root will be the lower bound on the delta-v of the transfer trajectory between the two halo orbits.

RESULTS AND EVALUATION OF APPROACH

The efficacy of this approach is evaluated in multiple ways. First, an example transfer trajectory is solved for by decomposing the motion using the IC method and then applying the previously referenced impulsive optimization algorithm developed by Koenig and D'Amico.[21] Second, the optimality of the delta-v cost found by the impulsive solver will be validated by comparison to delta-v lower and upper bounds found using the Jacobi Bounds method. Finally, the IC method is applied to the original CR3BP EOMs, prior to the Legendre polynomial expansion, to examine how the extraction of linear parts from higher order terms provides an advantage.

Example of Transfer Trajectory

This subsection illustrates the application of the impulsive solver described in the approach section and the quantitative and visual results it produces. The evolution of the spacecraft motion from the start to end of the transfer in both IC space and physical space is shown. Two arbitrary halo orbits with enough separation between them to easily visualize the transfer trajectory were chosen for this example. Table 1 summarizes the inputs and outputs of the impulsive optimization algorithm for those two halo orbits.

Table 1. Solved Transfer Trajectory

Parameter	Value
Initial Halo Orbit IC (DU)	[0.2229, 0, 0, 0, 1.0264, 0]
Target Halo Orbit IC (DU)	[0.2093, 0, 0, 0, 0.8088, 0]
Control Interval (TU)	[0, π]
Maneuver Times (TU)	[0.8885, 0.9203, 2.1579, 2.1896, 3.1416]
Total Delta-v Cost (km/s)	0.1490

Using the solved maneuver sequence, the change in IC space over time can be visualized in Figure 4. Each 2D subplot plots a pair of IC against each other. The IC are paired based on their geometric relationships, so the plot of C_1 vs C_2 gives insight into how the x and y amplitudes are changing, the plot of C_3 vs C_4 gives a sense of whether the divergent and convergent modes are active, and the plot of C_5 vs C_6 gives insight into how the z amplitudes are changing.

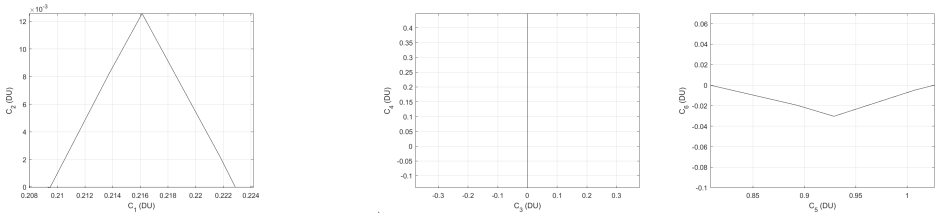

Figure 4. Change in IC space during transfer between halo orbits. Planar center modes C_1 vs C_2 (left), source/sink modes C_3 vs C_4 (right), and out-of-plane center modes C_5 vs C_6 (bottom).

Finally, the transfer trajectory can also be visualized in physical space as well. The transfer is represented in Figure 5 in both 3D and 2D views, and is displayed in RLPF coordinates.

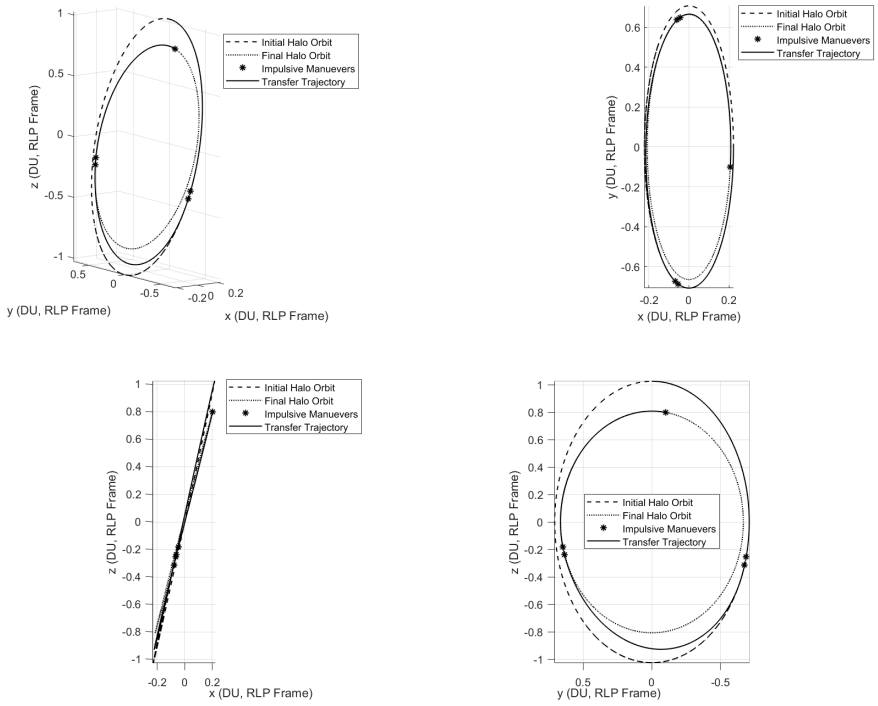

Figure 5. Change in physical space during transfer in RLPF coordinates. 3D view (top left), xy-plane (top right), xz-plane (bottom left), yz-plane (bottom right).

Generating this example trajectory demonstrates the functionality of the IC method for optimal control. The plots in Figures 4 and 5 showing the progression over time in IC and physical space give a visualization of the trajectory geometry. The next step is to evaluate the performance of the optimization algorithm.

Evaluation by Jacobi Bounds

To validate that the delta-v cost solved for by the optimization algorithm was of a reasonable magnitude, 40 transfer pairs were solved and compared to their respective Jacobi Bounds. For each transfer pair, the starting halo orbit had a z-amplitude of 667,500 km, which is among the smallest of the orbits generated for the Sun-Earth L2 family. The ending halo orbits varied in z-amplitude from 760,391 km to 1,823,661 km. This set of test cases was selected in order to give a wide range of ΔC_{goal}, as both the change in z-amplitude and ΔC_{goal} follow a similar trend. As stated previously, the difference between the two halo orbits in IC space, $\Delta \boldsymbol{C}_{goal}$ is defined as

$$\Delta \boldsymbol{C}_{goal} = \boldsymbol{C}_1 - \boldsymbol{C}_0 \tag{46}$$

For this work to be viable for use on missions such as ORCAS, a spacecraft must be capable of optimally transferring between orbits regardless of the required ΔC_{goal}, in order to align with

inertial targets at any declination. The results of the comparison of the solved delta-v to the Jacobi Bounds can be seen in Figure 6, which plots delta-v in km/s against the overall change in IC for the transfer, ΔC_{goal}.

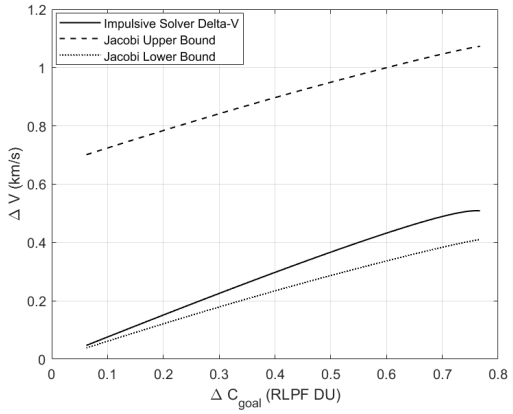

Figure 6. Comparison of Solved Transfer delta-v to Jacobi Bounds Over a Range of ΔC_{goal}

One key takeaway from Figure 6 is that the solved delta-v is not only within the Jacobi Bounds, but is consistently closer to the lower bound than the upper bound. The solved delta-v ranges from 0.009 km/s to 0.106 km/s greater than the lower bound, and 0.557 km/s to 0.654 km/s less than the upper bound. Also, the positive slope reflects how it usually takes more delta-v cost to transfer to halo orbits the greater the difference in both IC and z-amplitude size is between the two orbits. Finally, because the solved delta-v and Jacobi Bounds follow the same trend, it is conceivable that the lower bound could replace the solved delta-v in the cost function, or that either the upper or lower bound could be used to decide on the optimal order of halo orbits if needed for a multi-orbit trajectory, in lieu of the solved delta-v.

Comparison to Original EOMs

As a justification for performing the Legendre polynomial expansion, this subsection presents an examination of how the IC method would have worked if applied directly to the original CR3BP EOMs, which were introduced in expanded form in Equations (15)-(17). The linear, integrable part of the original CR3BP EOMs in matrix form is

$$\bar{\boldsymbol{F}}_1'(t,\boldsymbol{X}) = \dot{\bar{\boldsymbol{X}}}'(t) = \begin{bmatrix} \dot{\bar{x}} \\ \dot{\bar{y}} \\ \dot{\bar{z}} \\ \ddot{\bar{x}} \\ \ddot{\bar{y}} \\ \ddot{\bar{z}} \end{bmatrix} = \begin{bmatrix} 0 & 0 & 0 & 1 & 0 & 0 \\ 0 & 0 & 0 & 0 & 1 & 0 \\ 0 & 0 & 0 & 0 & 0 & 1 \\ 1 & 0 & 0 & 0 & 2 & 0 \\ 0 & 1 & 0 & -2 & 0 & 0 \\ 0 & 0 & 0 & 0 & 0 & 0 \end{bmatrix} \begin{bmatrix} \bar{x} \\ \bar{y} \\ \bar{z} \\ \dot{\bar{x}} \\ \dot{\bar{y}} \\ \dot{\bar{z}} \end{bmatrix} \tag{47}$$

The fundamental solution matrix found when solving this linear system of ODEs is

$$\bar{\mathbf{\Psi}}(t) = \begin{bmatrix} \cos t & \sin t & -\sin t + t\cos t & \cos t + t\sin t & 0 & 0 \\ -\sin t & \cos t & -\cos t + t\sin t & -\sin t - t\cos t & 0 & 0 \\ 0 & 0 & 0 & 0 & 2 & 2t \\ -\sin t & \cos t & -t\sin t & t\cos t & 0 & 0 \\ -\cos t & -\sin t & -t\cos t & -t\sin t & 0 & 0 \\ 0 & 0 & 0 & 0 & 0 & 2 \end{bmatrix} \tag{48}$$

The mapping of IC to the original state vector in Equation (48) is lacking in multiple ways. Most notably, the $\bar{z}$ position and velocity only includes constant and secular terms, and does not include the oscillatory out-of-plane motion. This would make it difficult, if not impossible to generate approximations of three-dimensional CR3BP orbits, including halo orbits.

A second issue is the defective eigenfrequencies. In the new method introduced in this work, the eigenfrequency ω_1 in Equation (29) is equal to 2.048. This means that a halo orbit under this approximation completes slightly more than two periods in the same time it takes the CR3BP system of rotating masses to complete a single revolution, which is correct, as the average period of a Sun-Earth L2 halo orbit is about 180 days, roughly half the length of an Earth year.[10] Conversely, the center modes governing the $\bar{x}\bar{y}$-plane motion in columns one and two of the matrix in Equation (48) have an eigenfrequency equal to 1. This means that in this deficient version of the IC mapping, an orbit completes a period in the same time as the system, which is incorrect by about a factor of two.

As a result of the imperfections, the control accuracy suffers as well. The same test cases against the Jacobi Bounds performed in the previous subsection were conducted again by running the impulsive solver using the solution matrix in Equation (48). The results of this comparison of the solved delta-v to the Jacobi Bounds can be seen in Figure 7, which plots delta-v in km/s against the overall change in IC for the transfer, ΔC_{goal}.

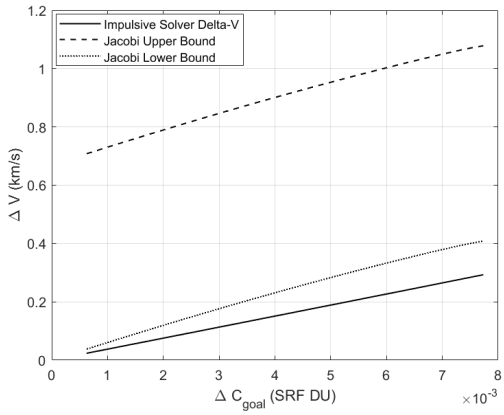

Figure 7. Comparison of Solved Transfer delta-v to Jacobi Bounds Over a Range of ΔC_{goal}

Figure 7 shows that the solved delta-v does not fall within the upper and lower bounds, which is not possible. This outcome reflects the poor accuracy of the simplified IC mapping, and underscores the improvement in control gained from better linearization.

In summary, the only closed orbit a linear mapping based on the original CR3BP EOMs would be able to trace out is a planar orbit with the wrong period. As a result, the ability to target specific orbits and configurations accurately would be greatly diminished. The actual approach put forth in this paper was able to form a better approximation of CR3BP dynamics by using the Legendre polynomial expansion, even while neglecting the non-integrable part. This allowed IC that had more geometric meaning to be obtained and used to achieve optimal control.

CONCLUSION

Orbit design in the Circular Restricted Three-Body Problem (CR3BP) is a promising avenue, due to the beneficial properties of halo orbits. Modern space missions, such as the Orbiting Configurable Artificial Star or the Orbiting Starshade, have different requirements than previous missions, and thus require innovative approaches beyond what the state-of-the-art currently offers. Reducing the reconfiguration costs associated with halo orbits will help allow them to be used in these types of missions. This paper took a first step towards using the integration constants method to develop an efficient and optimal way to transfer between halo orbits.

With the aid of Legendre polynomial expansion, the CR3BP equations of motion were split into linear and nonlinear parts. A set of integration constants (IC) was defined based on the closed-form map constructed by analytically integrating the linear part. Those IC served as state variables, which allowed the use of an impulsive solver to incorporate optimal control in IC space. The novel Jacobi Bounds method, which uses the energy properties of the CR3BP to determine upper and lower bounds on halo orbit transfers, was also introduced.

The transfer trajectory design process was demonstrated and then evaluated by comparison to the Jacobi Bounds method, which showed that the solved delta-v was valid. A comparison to the original equations of motion was also made to prove the necessity of the Legendre polynomial expansion and the clear improvements in control accuracy it provides.

Going forward, there are many ways to build on this work. The first priority would be incorporating more complexity into the equations of motion, so that the simulated motion more accurately reflects the actual dynamics. This means dropping simplifying assumptions and adding more perturbative or non-integrable terms, so that the complete Integration Constants Variation Equation (ICVE) can be used, thus unlocking the full potential of the IC method. The method could be applied iteratively to the ICVE in order to add higher order terms to the dynamics and rederive new IC. Ideally, the redefined CR3BP IC would incorporate more physical and geometric meaning, so that they could eventually be used in the same fashion as Keplerian and relative orbital elements.

ACKNOWLEDGEMENTS

This work was partially sponsored by the Air Force Office of Scientific Research (AFOSR) and Dr. Michael Yakes via award number FA9550-21-1-0414, for the project titled 'Autonomous Distributed Angles-Only Orbit Determination using Multiple Observers.'

REFERENCES

[1] E. Peretz, C. Hamilton, J. Mather, *et al.*, "Astrostationary Orbits for Hybrid Space and Ground-Based Observatories,"

[2] E. Peretz, J. Mather, R. Slonaker, J. O'Meara, S. Seager, R. Campbell, T. Hoerbelt, and I. Kain, "Orbiting configurable artificial star (ORCAS) for visible adaptive optics from the ground," *Bulletin of the American Astronomical Society*, Vol. 51, No. 7, 2019, p. 284.

[3] E. Peretz, C. Hamilton, J. C. Mather, L. Pabarcius, K. Hall, A. Michaels, R. Pritchett, W. Yu, P. Wizinowich, and E. Golliher, "ORCAS–Orbiting Configurable Artificial Star Mission Architecture," *UV/Optical/IR Space Telescopes and Instruments: Innovative Technologies and Concepts X*, Vol. 11819, International Society for Optics and Photonics, 2021, p. 1181905.

[4] A. W. Koenig, S. D'Amico, E. Peretz, W. Yu, S. Hur-Diaz, and J. Mather, "Optimal Spacecraft Orbit Design for Inertial Alignment with Ground Telescopes," *2021 IEEE Aerospace Conference (50100)*, IEEE, 2021, pp. 1–12.

[5] L. Hiday-Johnston and K. Howell, "Impulsive time-free transfers between halo orbits," *Celestial Mechanics and Dynamical Astronomy*, Vol. 64, No. 4, 1996, pp. 281–303.

[6] K. Howell and L. Hiday-Johnston, "Time-Free Transfers between Libration-Point orbits in the elliptic restricted problem," *Acta Astronautica*, Vol. 32, No. 4, 1994, pp. 245–254.

[7] L. Hiday-Johnston and K. Howell, "Transfers between libration-point orbits in the elliptic restricted problem," *Celestial Mechanics and Dynamical Astronomy*, Vol. 58, No. 4, 1994, pp. 317–337.

[8] G. Gómez, A. Jorba, J. Masdemont, and C. Simó, "Study of the transfer between halo orbits in the solar system," *NASA STI/Recon Technical Report A*, Vol. 95, 1993, pp. 623–637.

[9] J. Stuart, M. Ozimek, and K. Howell, "Optimal, low-thrust, path-constrained transfers between libration point orbits using invariant manifolds," *AIAA/AAS Astrodynamics Specialist Conference*, 2010, p. 7831.

[10] D. L. Richardson, "Analytic construction of periodic orbits about the collinear points," *Celestial mechanics*, Vol. 22, No. 3, 1980, pp. 241–253.

[11] T. Guffanti and S. D'Amico, "Integration Constants as State Variables for Optimal Path Planning," *2018 European Control Conference (ECC)*, IEEE, 2018, pp. 1–6.

[12] E. R. Burnett and H. Schaub, "Spacecraft Relative Motion Dynamics and Control Using Fundamental Solution Constants," *AIAA SCITECH 2022 Forum*, 2022, p. 2462.

[13] T. Guffanti and S. D'Amico, "Multi-Agent Passive Safe Optimal Control using Integration Constants as State Variables," *AIAA Scitech 2021 Forum*, 2021, p. 1101.

[14] M. Chernick and S. D'Amico, "Closed-form optimal impulsive control of spacecraft formations using reachable set theory," *Journal of Guidance, Control, and Dynamics*, Vol. 44, No. 1, 2021, pp. 25–44.

[15] K. C. Howell, "Three-dimensional periodic halo orbits," *Celestial mechanics*, Vol. 32, 1984, p. 53.

[16] W. Koon, M. Lo, J. Marsden, and S. Ross, "Dynamical Systems, The Three-Body Problem, and Space Mission Design," *Pasadena, CA, USA: California Institute of Technology*, 2006.

[17] A. J. Sinclair and J. E. Hurtado, "The motion constants of linear autonomous dynamical systems," *Applied Mechanics Reviews*, Vol. 65, No. 4, 2013.

[18] E. M. Zimovan, "Characteristics and Design Strategies for Near Rectilinear Halo Orbits Within the Earth-Moon System," Master's thesis, Purdue University, 2017.

[19] D. A. Vallado, *Fundamentals of astrodynamics and applications*, Vol. 12. Springer Science & Business Media, 2001.

[20] G. W. Hill, "Researches in the lunar theory," *American journal of Mathematics*, Vol. 1, No. 1, 1878, pp. 5–26.

[21] A. W. Koenig and S. D'Amico, "Fast algorithm for fuel-optimal impulsive control of linear systems with time-varying cost," *IEEE Transactions on Automatic Control*, Vol. 66, No. 9, 2020, pp. 4029–4042.